Inhibition of the RNA Regulator HuR mitigates spinal cord injury by potently suppressing post-injury neuroinflammation

Mohammed Amir Husain[1,6,7], Reed Smith[1,6,7], Robert E. Sorge[2,7], Abdulraheem Kaimari[1], Ying Si[1,6,7], Ali Z. Hassan[1], Abhishek Guha[1,6,7], Katherine A. Smith[1,6], Christopher P. Cardozo[8,9], Jennifer J. DeBerry[5,7], Shaida A. Andrabi[1,4], L. Burt Nabors[1], Natalia Filippova[1], Caroline K. Webb[2], Peter H. King**[1,3,6,7]

Departments of [1]Neurology, [2]Psychology, [3]Cell, Developmental, and Integrative Biology, [4]Pharmacology and Toxicology, [5]Anesthesiology and Perioperative Medicine, University of Alabama at Birmingham, Birmingham, AL, USA, 35294, [6]Center for Neurodegeneration and Experimental Therapeutics, University of Alabama at Birmingham, Birmingham, AL 35294; [7]Birmingham Veterans Affairs Medical Center, Birmingham, AL, 35294, [8]Spinal Cord Damage Research Center, James J. Peters VA Medical Center, Bronx, NY, [9]Department of Medicine, Icahn School of Medicine at Mount Sinai, New York, NY, USA,

**Correspondence to: Dr. P.H. King; UAB Dept. of Neurology, Civitan 545C, 1719 6th Ave South, Birmingham, AL 35294-0017, USA. Tel. (205) 975-8116; Fax (205) 996-7255; email: phking@uabmc.edu

Abstract

Background

Neuroinflammation plays a significant role in promoting secondary tissue injury after spinal cord trauma. Within minutes after spinal cord injury (SCI), microglia and astrocytes become activated and produce inflammatory mediators such as TNF-α, IL-6, iNOS and COX-2 which induce tissue injury through cytotoxicity, vascular hyperpermeability, and secondary ischemia. The inflammatory cascade is amplified by chemokines such as CCL2 and CXCL1 that promote recruitment of peripheral inflammatory cells into the injured spinal cord. HuR is a key post-transcriptional RNA regulator that controls glial expression of many pro-inflammatory factors by binding to adenylate- and uridylate-rich elements in 3' untranslated regions of the mRNA. SRI-42127 is a small molecule inhibitor that blocks HuR nucleocytoplasmic translocation, a process critical for its regulatory function. The goal of this study was to assess the potential of SRI-42127 for suppressing neuroinflammation after SCI and improving functional outcome.

Methods

Adult female mice underwent a contusion injury at the T10 level. SRI-42127 or vehicle was administered intraperitoneally starting 1 h after injury and up to 5 days. Locomotor function was assessed by open field testing, balance beam and rotarod. Immunohistochemistry was used to assess lesion size, neuronal loss, myelin sparing, microglial activation and HuR localization. Molecular analyses of spinal cord and peripheral tissues for expression of inflammatory mediators included qPCR, immunohistochemistry, ELISA, or western blot. Post-SCI pain was assessed by the mouse grimace scale.

Results

SRI-42127 significantly attenuated loss of locomotor function and post-SCI pain. Histologic correlates to these beneficial effects included reduced lesion size, neuronal loss, and an increase in myelin sparing. There was reduced microglial activation at the epicenter with concomitant

attenuation of HuR nucleocytoplasmic translocation. Molecular analysis revealed a striking reduction of pro-inflammatory mediators at the epicenter including IL-6, MMP-12, IL-1β, TNF-α, iNOS, COX-2, and chemokines CCL2, CXCL1, and CXCL2. Suppression of inflammatory responses extended peripherally including serum, liver, and spleen.

Conclusion

Targeting HuR after SCI is a viable therapeutic approach for suppressing neuroinflammatory responses after tissue injury and improving functional outcome.

KEYWORDS

SRI-42127, Spinal cord injury, HuR translocation, neuroinflammation, RNA regulation

Background

Traumatic spinal cord injury (SCI) is a debilitating neurological injury affecting more the 250,000 individuals per year globally. The injury often results in in permanent disability and shortened lifespan. Additionally, there are life-changing socioeconomic consequences for both the individual and their caregivers, particularly younger people [1, 2]. Treatment in the acute phase of injury is mainly supportive with limited treatment options for neuroprotection to improve recovery and reduce long term disability.

The physical trauma of SCI triggers a robust inflammatory response initiated within minutes by resident microglia and astrocytes in the vicinity of tissue injury. This activation leads to production of pro-inflammatory mediators including IL-1β, IL-6, TNF-α, MMPs, COX-2 and nitric oxide (NO) via iNOS that exert direct toxic effects on neurons, oligodendroglia, and endothelial cells, often leading to apoptosis and peaking within the initial 24 h post injury [3, 4]. These mediators increase vascular permeability by disrupting the blood-spinal cord barrier (BSCB), leading to edema, secondary ischemia, and hemorrhage [5, 6]. Disruption of the BSCB, in combination with glial secretion of chemokines such as CCL2 and CXCL1, further intensifies the inflammatory cascade by facilitating recruitment and infiltration of peripheral neutrophils and monocytes [3].

An integral regulatory component to this inflammatory cascade, beginning with activated microglia and astrocytes, is at the posttranscriptional level, where AU-rich elements (ARE) in the 3' untranslated region (UTR) of pro-inflammatory mRNAs govern their expression through modulation of mRNA stability and translational efficiency [4]. HuR, a major cellular RNA-binding protein (RBP) in glial cells, binds to these AREs and positively regulates the stability and translational efficiency leading to increased expression [4, 7-10]. Primarily located in the nucleus, HuR translocates to the cytoplasm upon activation where it transports and stabilizes bound

102 mRNAs and facilitates their localization to polysomes for translation. In microglia and/or
103 astrocytes, HuR translocation is triggered in different inflammatory conditions, including SCI [9,
104 11], amyotrophic lateral sclerosis [8], lipopolysaccharide (LPS) stimulation [10, 12], hypoxia [10],
105 and glioblastoma [7]. Knockdown or deletion of HuR in microglia or astrocytes significantly
106 diminishes the expression of many key inflammatory mediators, including pro-inflammatory
107 cytokines, chemokines, and iNOS, associated with secondary tissue injury in SCI [7-9]. Our group
108 has recently developed a small molecule, SRI-42127, that blocks HuR dimerization, a process
109 critical for cytoplasmic shuttling and RNA binding [13-15]. SRI-42127 inhibits translocation of HuR
110 in microglial cells and astrocytes after activation with LPS and suppresses the production of pro-
111 inflammatory mediators [10]. In our prior work, SRI-42127 potently attenuates development of
112 neuropathic pain in a peripheral nerve injury model, a process that is driven by neuroinflammatory
113 responses in the spinal cord [16, 17]. With this background, we hypothesized here that inhibition
114 of HuR with SRI-42127 would suppress neuroinflammatory responses after acute SCI, reduce
115 secondary tissue injury, and mitigate loss of motor function.
116
117

118 **Methods**

119

120 **Animals and contusion model of spinal cord injury**

121 All animal procedures were approved by the UAB Institutional Animal Care and Use Committee
122 and were carried out in accordance with relevant guidelines and regulations of the National
123 Research Council Guide for the Care and Use of Laboratory Animals. Female C57/Bl6 mice
124 between 10–14 weeks of age were anesthetized under isoflurane and a laminectomy was
125 performed to remove the dorsal aspect of the T10 vertebrae. The animal was transferred to a
126 spinal stereotaxic frame and clamps were attached to the T9 and T11 vertebral spines to secure
127 the vertebral column. Using a 0.8-mm diameter tip, a single impact contusion of 50 kdyn was
128 delivered using the Infinite Horizon spinal cord injury device (Precision Systems &
129 Instrumentation, Lexington, KY). Sham control mice received a laminectomy only. Post-
130 operatively, animals received manual bladder evacuation twice daily to prevent urinary tract
131 infections. One dose of subcutaneous buprenorphine was administered prior to injury and every
132 12 h for 3 d post injury. For molecular studies, SRI-42127 (10 mg/kg) and vehicle were prepared
133 as previously described [16] and administered intraperitoneally every 2 h beginning 1 h after injury
134 for 4 doses. The cohort for behavioral studies received 4 doses daily, starting 1 h after injury, for
135 5 days.

136

137 **RNA isolation and qPCR**

138 The thoracic spinal column was harvested, and 2 mm sections were cut from the epicenter of
139 injury and adjacent rostral, caudal spinal column. Spinal cord was removed from these sections
140 and RNA was isolated using TRIzol reagent as per manufacturer's protocol (Thermo Fisher
141 Scientific). RNA was precipitated using isopropanol (Sigma) and glycogen (Thermo Fisher
142 Scientific) and concentrations were measured by Nanodrop (Thermo Scientific, Waltham, MA).
143 Complementary DNA was reverse transcribed from 2 μg of total RNA using a reverse transcription

144 kit (Thermo Fisher Scientific). Quantitative Real Time PCR (qRT-PCR) was conducted using the
145 ViiA7-Real-Time PCR system and primers and probes from Applied Biosystems as previously
146 described [10].
147
148 **Western blot and ELISA**
149 For western blotting, whole cells lysates were prepared using T-PER (Thermofisher) and
150 quantification was done with a BCA protein assay kit (Thermofisher). Fifty µg of protein per sample
151 were electrophoresed in 4%–20% mini-PROTEAN gel (Biorad) and transferred to a nitrocellulose
152 membrane. Blots were immunostained with a COX-2 antibody (Santa Cruz Biotechnology, USA
153 Inc) was used at a dilution of 1:1000. Each sample was analyzed in triplicate and quantified using
154 Image lab software (Bio-Rad Laboratories, USA Inc.). For ELISA of peripheral serum samples,
155 cytokines (IL-1β, IL-6, IL-10, TNF-α, CCL2, CXCL1) were measured using U-plex biomarker
156 Group 1 (mouse) Assays (K15069M, MSD). Analyses were done using a QuickPlex SQ 120
157 instrument (MSD) and DISCOVERY WORKBENCH® 4.0 software (MSD).
158
159 **Immunohistochemistry**
160 Mice were euthanized 8 h or 3 weeks and perfused with an ice-cold phosphate buffer saline (PBS)
161 solution for 2 min followed by 4% paraformaldehyde (PFA) solution for 5 min [9]. The entire spinal
162 column was then extracted and post-fixed in PFA for 24 h before being decalcified with 8%
163 hydrochloric acid and 10% ethanol in PBS. The spinal column was incubated in a PBS solution
164 with 10% sucrose for cryoprotection then transferred to a 30% sucrose in PBS solution for 48 h.
165 Two mm samples of the spinal column from epicenter and adjacent rostral (+ 2 mm) and caudal
166 tissues (- 2 mm) were preserved and cryo-molded in OCT. A cryostat was used to cut samples
167 into 30 µm serial sections cut transversely.
168 Sections were washed with PBS and blocked in 10% goat serum for 1 h. Samples were incubated
169 overnight with primary antibodies (GFAP, 1:500, Z0334, Dako, Carpinteria, CA), (Iba1, 1:500,

170 FUJIFILM Wako Chemicals U.S.A. Corporation), (NeuN, 1:400, ABN78, Sigma-Aldrich, USA
171 Ltd.), (HuR, 1:500, sc-5261, Santa Cruz Biotechnology, USA Inc). The following day, slide
172 sections were washed and incubated with Alexa fluorophore-conjugated secondary antibodies
173 (Goat anti mouse, A28175, Thermo Fisher Scientific and Goat anti rabbit Cy3, 111-165-144,
174 Jackson Immuno Research) for 2 h, mounted with antifade DAPI + mountant (ThermoFisher
175 Scientific P36966). For myelin staining, sections were incubated with FluoroMyelin Green for 20
176 minutes (1:300, Invitrogen).
177 Quantitative assessment of HuR localization was done using our previously published method
178 [10]. Fiji software was utilized for image analysis, and a minimal threshold was established in
179 order to quantify the mean fluorescence intensity (FI). FI was quantified and normalized with the
180 DAPI FI for the same region and expressed as arbitrary units (AU). Total lesion area was
181 determined based on the ratio of GFAP-stained area (which is concentrated on the border of the
182 injured region) to total spinal cord area. The total area of GFAP and myelin staining was measured
183 using the freehand selection tool and threshold functions in Fiji. Three biological replicates were
184 used for the Fiji analysis.
185
186 **Analysis of microglial morphology**
187 During the early stages of activation, microglia can become hyper-ramified with increase branch
188 complexity and soma enlargement [18, 19]. Fiji software (https://imagej.net/) was used to convert
189 all photomicrographs to binary and skeletonized images using AnalyzeSkeleton plugin
190 (https://imagej.net/plugins/analyze-skeleton/). To analyze the number of branches, the total
191 branch length, and the endpoints per microglia brightness and contrast are changed by updating
192 the Fiji lookup table, so pixel values are unchanged. This is followed by a despeckle step to
193 remove salt-and-pepper noise. Photomicrographs then converted to binary using threshold tool
194 followed by skeletonizing the image using the toolbar Skeletonize and AnalyzeSkeleton (2D/3D)
195 to collect data on the branch length. Branch length per cell was calculated by dividing summed

196 branch length by the number of microglia somas in the corresponding photomicrographs. Data
197 was obtained from 5007 microglial cells from vehicle control (n=3) and 4538 microglial cells from
198 SRI (n=3). The soma area was calculated using the Fiji multipoint area selection tool.
199
200 **Open field test**
201 Motor function of the hind limbs was scored at 1, 2 and 3 weeks after SCI using the open-field
202 basso mouse scale (BMS) in 10 min observation periods. BMS is a reliable measure and has
203 been widely used to evaluate motor functions after SCI in mice [20]. Briefly, each mouse was
204 separately placed in an open field (60 cm x 120 cm) and patterns of limb movement such as ankle
205 movement, plantar placing and stepping of paw, paw positions and trunk instability were recorded
206 over a 10 min time interval by a ceiling camera and analyzed by a computerized tracking system
207 EthoVision XT sofware (Noldus, USA). Prior to the testing day, baseline measurements were
208 obtained. Videos were carefully inspected by two reviewers (MAH and HAZ) blinded to the
209 experimental conditions. Hindlimb joint movement, coordination, and weight support were
210 evaluated using a rating scale from 0 points (no movement of any kind) to 9 points (normal
211 locomotion). EthoVision software was used to analyze recorded videos to automatically calculate
212 total distance traveled, mobility and velocity by each mouse within the arena.
213
214 **Beam walking**
215 The apparatus consists of a round horizontal beam of 100 cm long and 1.2 cm in diameter and
216 was elevated 50 cm above the ground. A hollow black escape box was attached to one end of
217 the beam. One fluorescent lamp (60W) was used to illuminate the beam from the start side. One
218 week prior to SCI, mice were thoroughly trained to traverse the beam from start point to end point
219 (black box). Baseline measurements were taken one day before the SCI. On the trial days after
220 SCI mice were placed at the start point and were allowed to walk for 2 min for 3 trials. The test
221 was recorded by video camera. A scoring was given to the mice as described elsewhere [21].

222 Briefly, the rating system employs values such as mouse retention, forward motion, and goal-
223 achieving on a beam. Mice received a high score for effectively using its hindlimbs to move around
224 the beam. In case of absence of hindlimb movements, mice received no points. Scoring was done
225 by an observer blinded to the identity of the mouse using recorded video weeks 1, 2, and 3 after
226 SCI. A mean value was calculated from the three trials for each mouse.
227
228 **Rotarod**
229 Motor coordination was assessed in weeks 1, 2, and 3 post SCI on an accelerating rotarod (San
230 Diego instruments CA, USA). Mice were trained one week before SCI by placing them on the
231 revolving rotor (4 rpm) and allowing them to acclimate for 2 mins. Baseline measures were
232 acquired one day prior to the contusion injury. On the day of testing day, the rod accelerated from
233 4 to 60 rpm over 2 mins and the latency to fall off was measured in 2 trials on each testing day,
234 allowing them 5 minutes of rest with in between each trial. The average time for the 2 trials was
235 used for statistical analysis to calculate a single score for each mouse.
236
237 **Non-evoked Pain testing**
238 Mice were placed into tabletop plexiglas cubicles (12 x 8 x 5.5 cm) with perforated metal floors
239 and clear walls. High-resolution (1920x1080) cameras (Sony Handycam model HDR-CX100)
240 were set up in front and behind the cubicles as described elsewhere [22]. After 15 min of
241 habituation, cameras were turned on to record for 15 mins. Recordings were taken prior to surgery
242 (baseline, BL) and at days 2 and 9 post SCI. Still images with clear visuals of the face were taken
243 once in each 2-minute period for each recording (8 images total) by an experimenter blinded to
244 the group assignment. Images were added to a PowerPoint file, randomized, and scored by two
245 experimenters blinded to the experimental conditions. Scores for action units were averaged
246 within each recording session. Action unit scores were averaged to calculate a mouse grimace
247 score (MGS).

248

249 **Statistics**

250 All statistical analyses were performed by Graphpad (GraphPad Software Inc.). The mean values
251 are shown on graphs along with error bars. Error bars indicate the standard deviation and
252 standard error as indicated. An unpaired Welch's t test was used for HuR localization, qPCR,
253 western blot, FI, and microglia counting. Two-way ANOVA with Tukey post hoc test was used for
254 CCR2. Data from all behavioral testing were analyzed using an unpaired Welch's t test. A p-value
255 less than 0.05 was considered statistically significant.

256

257

258

Results

SRI-42127 treatment improves functional recovery after SCI

Wild-type female mice were subjected to a mid-thoracic contusion injury and then treated with SRI-42127 every 6 h for 5 days, starting 1 h after injury. To assess and quantitate motor activity over a longer period of time, we used a computerized tracking system in an open field **(Fig. 1A-E)**. We first assessed locomotor function using the Basso mouse scale (BMS) at weeks 1, 2, and 3 post SCI **(Fig. 1A)**. There was a highly significant increase in BMS scores for SRI-treated mice versus vehicle beginning at week 1 (4.2 ± 1.2 versus 0.2 ± 0.1; $P < 0.0001$). The separation of BMS scores persisted and remained significant in weeks 2 and 3 with both groups showing some recovery by week 3. Heat maps of activity within the field were generated (example shown in **Fig. 1B**) from which distance moved, mobility and velocity were calculated **(Fig. 1C, D, E)**. At week 1, there was more than a two-fold increase in distance moved (3900 ± 200 versus 1800 ± 100 cm; $P < 0.0001$), mobility (6.5 ± 0.7 versus 4.0 ± 0.5 percent; $P = 0.0029$), and velocity (6.8 ± 1.0 versus 3.0 ± 0.5 cm/sec; $P < 0.0001$). The differences between SRI- and vehicle-treated groups remained significant throughout the recovery period for each parameter with both groups showing improvement by week 3. We next assessed the animals with a novel beam walking test which quantitates locomotor recovery using a scale of 0 to 7 **(Fig. 1F)** [21]. This test provides a more comprehensive assessment of beam walking by measuring other functional components besides latency to reach the other side. In both test groups, pre-injury baseline (BL) scores were 7. At week 1, there was a significant increase in score in the SRI-treated group compared to vehicle (3.3 ± 1.2 versus 0.6 ± 0.2; $P < 0.0001$). This difference persisted throughout the three-week observation period, with both groups showing modest improvement by week 3 (5.0 ± 1.2 versus 2.0 ± 0.5; $P < 0.0001$). Next, we assessed rotarod performance **(Fig. 1G)** and found that SRI-treated mice had a ~5-fold increase in mean latency to fall at week 1 compared to vehicle control (6.8 ± 3.1 versus 1.3 ± 1; $P = 0.0012$). This difference remained significant throughout the recovery

285 period with both groups showing increases in latency by week 3. To exclude the possibility of a
286 drug effect on motor function, independent of SCI, we performed open field testing, BMS, and
287 beam walking on sham-injured mice given SRI-42127 and observed no difference compared to
288 the vehicle group over the 3-week testing period **(Supplementary Fig. 1)**. Since pain is a common
289 and debilitating sequelae of SCI, we assessed non-evoked pain using the mouse grimace scale
290 (MGS) **(Fig. 1H)**. At baseline, prior to SCI, the groups had similar MGS scores (0.31 ± 0.02 versus
291 0.29 ± 0.04). Following SCI, mice treated with SRI-42127 had significantly lower MGS scores
292 when compared to vehicle-treated mice (day 2: 1.56 ± 0.11 versus 1.02 ± 0.09, $p < 0.01$; day 9:
293 0.83 ± 0.08 versus 0.46 ± 0.05, $p < 0.01$). Taken together, SRI-42127 treatment after SCI
294 significantly attenuated motor function loss and pain.
295
296 **SRI-42127 mitigates histopathology after SCI**
297 At 3 weeks post SCI, spinal cords were harvested and tissue sections at the epicenter and
298 adjacent rostral and caudal levels to assess for histopathological changes. To identify the glial
299 scar border, we immunostained sections with GFAP **(Fig. 2A)**. Using these borders, a lesion size
300 was calculated and found to be reduced by 60% in SRI-treated mice versus vehicle (P = 0.003)
301 **(Fig. 2B)**. Inspection of rostral and caudal levels revealed no evidence of glial scar
302 **(Supplementary Fig. 2A)**. To assess for neuronal loss, sections were immunostained with NeuN
303 **(Fig. 2C)**. In SRI-treated mice, there was a 7-fold increase in NeuN positive cells in the epicenter
304 (**Fig. 2D**; P= 0.003**)**. Overall NeuN fluorescence intensity (FI) was significantly higher in SRI-
305 treated mice **(Fig. 2E)**. In rostral and caudal levels, there were no differences in NeuN FI in SRI-
306 and vehicle-treated mice **(Supplementary Fig. 2B)**. To assess white matter sparing at 3 weeks
307 in SRI-treated mice compared to vehicle controls (**Fig 2F, G**; *P* = 0.003). In rostral and caudal
308 post SCI, spinal cord sections were stained with fluoromyelin. There was a 4.5-fold increase in FI
309 levels, there was also a significant 40-50% increase in FI in SRI-treated mice (**Supplementary**
310 **Fig. 2C**).

311

312 **SRI-42127 blocks nucleocytoplasmic translocation of HuR in microglia and attenuates**
313 **microglial activation**

314 A hallmark of HuR activation is its translocation from nucleus to the cytoplasm where it stabilizes
315 and promotes the translational efficiency of pro-inflammatory mediators in microglial cells [4, 10].
316 Here we assessed HuR localization by immunohistochemistry in Iba1+ cells at 8 h post SCI. At
317 the epicenter, there was prominent HuR translocation in vehicle-treated mice, as indicated by a
318 merged signal with cytoplasmic Iba1 (**Fig. 3A**). This shift was not seen in uninjured rostral or
319 caudal levels (**Supplementary Fig. 3**). In SRI-treated mice, this merged signal was not observed
320 (**Fig. 3B**). A nuclear/cytoplasmic ratio of HuR FI was calculated and found to be more than 2-fold
321 higher in SRI-treated mice (P = 0.008) consistent with nuclear retention of HuR (**Fig. 3C**). To
322 assess microglial activation, we measured Iba1 FI for individual cells in the epicenter and found
323 an overall reduction consistent with reduced activation (**Fig. 3D**). This was underscored by a
324 reduction in total Iba1 FI at the epicenter in SRI-treated mice (**Fig. 3E**) since the overall Iba1+ cell
325 count was unchanged (**Fig. 3F**). Iba1 FI in rostral and caudal segments showed no differences
326 between SRI-treated and vehicle control mice (**Fig. 3E**). Interestingly, we did not see translocation
327 of HuR in astrocytes in vehicle-treated mice at this early timepoint but did at 24 h (**Supplementary**
328 **Fig. 4A versus 4B**). In summary, these findings indicate prominent HuR cytoplasmic
329 translocation in microglia (and astrocytes) after SCI which is suppressed with SRI-42127
330 treatment.

331

332 **SRI-42127 attenuates activation-associated microglia morphological changes**

333 As another measure of activation, we assessed morphological changes of microglia at the
334 epicenter 8 h after SCI. Using Fiji software, a skeleton analysis of microglia was done as
335 previously described [23] (**Fig. 4A**). We observed a decrease in branch length (P = 0.009),

336 number of branches ($P < 0.0001$), and number of end points per microglia ($P < 0.0001$) in drug-
337 treated mice, consistent with reduced early-stage activation [24]. In addition to hyper-
338 ramification, we measured soma size as an indicator of reactive microglia and found a significant
339 reduction in SRI-treated mice (**Fig. 4B**; $P < 0.0001$). Taken together with results in Fig. 3, SRI-
340 42127 attenuates microglial activation after SCI.
341
342 **SRI-42127 suppresses induction of proinflammatory mediators at the epicenter of SCI**
343 At 8 h post-SCI, spinal cords were harvested and divided into 3 segments: injury epicenter, rostral
344 and caudal. RNA expression of proinflammatory mediators was assessed by qPCR. At the
345 epicenter, there was a large induction of *IL-6*, *IL-1β*, *TNF-α*, *CCL2*, *MMP12*, *CXCL1*, *CXCL2*, and
346 *iNOS* in the vehicle control compared to rostral and caudal segments (**Fig. 5A**). *COX2 and TGF-*
347 *β1* mRNAs were not induced. The induction was most pronounced with *IL-6* (34-fold) and *CXCl2*
348 (39-fold) while the others ranged from 5- to 15-fold. SRI-42127 treatment suppressed the
349 expression of all pro-inflammatory mediators, most potently for *IL-6* (~13-fold) and *IL-1β* (~9-fold).
350 Other inflammatory mediators were suppressed by 3- to 7-fold. Interestingly, there was SRI-
351 induced suppression of some mRNAs at non-injured spinal cord segments, including *IL-1β*, *CCL2*,
352 *MMP-12*, and *CXCL1*. Based on our prior work showing that HuR positively regulates *CCR2* in
353 microglia [8], we assessed this mRNA after injury and found a nearly 3-fold attenuation at the
354 epicenter. SRI-42127 suppressed *CCR2* mRNA at the uninjured levels as well. The fold-change
355 was even larger as there was significantly higher expression of *CCR2* in non-injured levels for the
356 vehicle control. Since COX-2 is heavily regulated by HuR at the translational efficiency level in
357 addition to mRNA stability [25, 26], we assessed protein levels by western blot (**Fig. 5B**). We
358 found a 2-fold increase in COX-2 protein levels in vehicle-treated mice compared to uninjured
359 levels and this was attenuated by ~4-fold in SRI-treated animals.
360

361 To determine the impact of SRI-42127 on inflammatory cytokine induction at a later timepoint, we
362 assessed spinal cords after five days of SRI-42127 or vehicle treatment (**Supplementary Fig. 5**).
363 There was a sustained suppression of pro-inflammatory mediators, most potently for *MMP-12*
364 (~90-fold) and *CXCl2* (~30-fold). Others were suppressed by 3- to 9-fold. *TGF-β1*, on the other
365 hand, was greater in vehicle-treated mice by ~3-fold. No difference was seen with *IL-1β* while
366 *CXCL1*, *iNOS*, and *COX-2* trended toward suppression but did not reach significance due to
367 higher variability of mRNA levels. Taken together, treatment with SRI-42127 in the acute phase
368 of SCI broadly suppressed the induction of pro-inflammatory mediators at the level of injury.
369

370 **SRI-42127 attenuates peripheral inflammatory responses after SCI**

371 We next examined the effects of SRI-42127 on peripheral inflammatory responses at 8 h post
372 SCI (**Fig. 6**). We first looked at circulating levels of key inflammatory mediators and found a large
373 increase in IL-6 (5.8 vs. 6719 pg/ml) and CXCL1 (32.7 vs 3268) in vehicle-treated mice after SCI
374 compared to sham-injured mice (**Fig. 6A**). CCL2 also increased by 3-fold (77.2 vs 226 pg/ml).
375 With SRI-42127 treatment there was a significant attenuation of these inflammatory mediators:
376 IL-6 (~5-fold; $P < 0.0001$), CXCL1 (~3.5-fold; $P < 0.0001$) and CCL2 (~2.5-fold; $P = 0.003$). While
377 there was some increase in IL-10, TNF-α, and IL1-β in vehicle-treated mice after SCI compared
378 to sham-injured mice, SRI-42127 did not suppress this increase. To gain insight into potential
379 sources for these cytokines, we looked at liver and spleen, two organs that drive the influx of
380 inflammatory macrophages (**Fig. 6B**) [27, 28]. In liver tissue, we observed a significant induction
381 of *CXCL1* (~16-fold) and *IL-6* (9-fold) mRNA which was suppressed by ~16-fold and 11-fold,
382 respectively, with SRI-42127 treatment. For splenic tissue, there was an increase in *CCL2* (~16-
383 fold) and *IL-6* (~10-fold) mRNA expression which was suppressed by ~16-fold and ~8-fold,
384 respectively, with SRI-42127 treatment. For cytokines that were not elevated in serum, including
385 IL-1β, TNF-α, and IL-10, there was only minimal induction of TNF-α in liver compared to sham
386 injury **(Supplementary Figure 6)**.

387

388 **Discussion**

389 A major challenge in therapeutically targeting the inflammatory cascade after SCI is the
390 heterogeneity and complexity of signaling pathways driven by a broad range of pro-inflammatory
391 mediators induced after injury [3, 29, 30]. These pathways are numerous, often overlapping, and
392 orchestrated by many cell types at different stages of acute injury including microglia,
393 macrophages, neutrophils, and astrocytes [30, 31]. HuR is a major RNA regulator of many pro-
394 inflammatory mediators and is expressed in these cell types, making it a rational target for
395 maximizing suppression of multiple components in the inflammatory cascade [3, 4, 7, 30, 32, 33].
396 In this report, we have shown that inhibiting HuR with the small molecule SRI-42127 potently
397 suppresses pro-inflammatory responses in the spinal cord and periphery in the acute phase of
398 SCI, resulting in a significant attenuation of motor function loss and pain. Histologic correlates for
399 this therapeutic effect include sparing of neurons and whiter matter at the level of injury, reduced
400 lesion size, and reduced microglial activation.

401

402 A deleterious effect of glial HuR in SCI was first reported by our group using a transgenic mouse
403 model where its selective overexpression in astrocytes accentuated spinal cord edema, neuronal
404 loss and neuroinflammatory responses after acute injury [9, 11]. In those reports, we described
405 prominent nucleocytoplasmic translocation of both endogenous (and transgenic) HuR similar to
406 what we observed in microglia and astrocytes in the current work. In glial cells, HuR is
407 predominantly nuclear in localization, but upon activation by triggers such as LPS [10], hypoxia
408 [10], glioblastoma [7, 32], and amyotrophic lateral sclerosis [8], translocates to the cytoplasm to
409 promote mRNA stabilization and translational efficiency of pro-inflammatory mediators [4, 32].
410 HuR translocation was prominent in microglia/macrophages and astrocytes at the epicenter early
411 of injury, but not rostrally or caudally, indicating a specificity of activation to the level of trauma. In

412 astrocytes, HuR translocation occurred by 24 h post SCI, consistent with our previous reports [9,
413 11], but not at 8 h, suggesting that microglial HuR is activated earlier on in SCI. In both cell types,
414 however, SRI-42127 attenuated cytoplasmic HuR which is consistent with its mechanism of
415 blocking HuR dimerization [10, 13-15].
416
417 Inhibition of HuR with SRI-42127 led to a striking suppression of two cytokines, IL-6 and IL-1β, at
418 the epicenter, both of which are rapidly induced within 1-3 hours after injury [29]. These cytokines
419 are considered key initiators of the inflammatory cascade and directly produce toxic effects on
420 neurons, oligodendrocytes, endothelial cells, leading to apoptosis and necrosis [30]. They are
421 mainly produced by microglia and astrocytes activated upon exposure to damage associated
422 molecular patterns (DAMPs) produced by the injury [4, 30]. This profound suppression was
423 consistent with our prior studies indicating that SRI-42127 had the greatest suppressive effect on
424 IL-1β and IL-6 induction in primary microglia and astrocytes *in cellulo* after LPS stimulation, and
425 spinal cord microglia *in vivo* after spared nerve injury (SNI) [10, 16]. In the SNI model, SRI-42127
426 treatment significantly reversed allodynic pain in acute and chronic phases of the injury [16]. IL-6
427 and its signaling pathway are causally linked to neuropathic pain in SCI [34-36]. In prior reports,
428 blocking the pathway with a neutralizing antibody to the IL-6 receptor or inhibiting the downstream
429 transducer, JAK2, abrogated the development of pain and improved functional recovery. Thus,
430 the early and marked suppression of IL-6 in the epicenter of SRI-treated mice may underlie the
431 significant attenuation of spontaneous pain observed after SCI.
432
433 SRI-42127 suppressed other pro-inflammatory mediators in the initial 8 h post injury that further
434 enhance the inflammatory cascade and toxic microenvironment via different pathways, including
435 iNOS (via nitric oxide), COX-2 (via PGE_2), and MMP-12 [3, 29, 30, 37, 38]. Interestingly COX-2
436 protein but not mRNA was suppressed with SRI-42127 treatment. This may be related to a loss
437 of translational efficiency rather than mRNA stability (and decrease in mRNA levels) as both

438 processes represent two distinct posttranscriptional levels of regulation governed by HuR [4]. We
439 have shown previously that these mediators are regulated by HuR in glial cells in different
440 inflammatory environments and suppressed either by SRI-42127, MS-444 (another chemical HuR
441 inhibitor [15]) or with HuR silencing/deletion [7-10, 16, 39]. In addition to direct toxic effects, these
442 inflammatory mediators also trigger indirect toxicity by promoting vascular permeability, edema,
443 ischemia, and hemorrhage [1, 30].
444
445 In the acute phase of injury, the inflammatory cascade is further amplified by glial and macrophage
446 production of chemokines, particularly CXCL1, CXCL2 and CCL2 which promote recruitment and
447 activation of neutrophils, monocyte/macrophages, and other immune cells from the periphery [1,
448 30]. These chemokines were likewise suppressed by more than 6-fold with SRI-42127 treatment.
449 In a compressive model of SCI, depletion of CCL2+ microglia significantly attenuated neuropathic
450 pain [40]. CCL2-depeleted microglia switched from a pro- to anti-inflammatory phenotype and
451 demonstrated reduced migration and invasion properties. CCL2 also can activate spinal microglia
452 when injected intrathecally and trigger behavioral patterns consistent with neuropathic pain [41].
453 Interestingly, our prior work showed that HuR is a major positive regulator of CCR2, the main
454 receptor for CCL2, in microglia and macrophages [8]. This is consistent with the >60% attenuation
455 of *CCR2* mRNA levels at the epicenter with SRI-42127 treatment. *CCR2* knockout abrogates
456 neuropathic pain after nerve injury which may tie into the attenuation of pain observed here [42,
457 43]. Of note, the fold-suppression of *CCR2* mRNA with drug treatment was even greater at rostral
458 and caudal levels (~6-fold) due to the higher expression of *CCR2* mRNA in vehicle controls at
459 those levels. This difference is likely due to injury-related loss of neurons, astrocytes and
460 oligodendrocytes, all of which express CCR2 [44].
461
462 Interestingly, *TGF-β1* was not induced at 8 h post injury or altered with SRI-42127 treatment but
463 increased by ~5-fold in vehicle-treated mice at 5 days. This timeframe is consistent with a prior

464 report where TGF-β1 induction occurred more gradually (over days) after SCI [45]. In prior *in vivo*
465 studies, we did not see suppression of TGF-β1 in brain or spinal cord tissues in SRI-treated mice
466 [10, 16] and so the increase observed here may relate to enhanced glial scar signaling pathways
467 due to a larger lesion size. TGF-β1 promotes astrocyte proliferation and glial scar formation and
468 the 5-day timepoint represents the early stage of that process [46-48].
469
470 In SCI (and other forms of CNS trauma), there is a rapid peripheral response in organs such as
471 liver and spleen that strongly influences the pro-inflammatory microenvironment in the injured
472 cord by promoting mobilization and recruitment of inflammatory monocyte/macrophages and
473 neutrophils [27, 28, 49-52]. In liver and spleen there is production and release of chemokines
474 CXCL1 and CCL2 that drive this recruitment. Consistent with prior reports [50, 52], we observed
475 a significant increase in circulating CXCL1 at the early timepoint of 8 hours post injury with liver
476 tissue showing a ~15-fold induction of *CXCL1* mRNA. SRI-42127 potently suppressed both
477 hepatic mRNA induction and circulating levels of CXCL1. Although early induction of *CCL2* in liver
478 has been observed with compression spinal cord injury models and later time points [51, 53], we
479 did not see this at 8 hours in our model. On the other hand, circulating CCL2 levels were increased
480 and spleen tissue showed a selective ~15-fold induction of *CCL2* mRNA. A prior report identified
481 spleen as the major source for monocyte-derived macrophages recruited to the injured spinal
482 cord and pre-SCI splenectomy led to improved recovery [54].The induction of CCL2 after SCI was
483 attributable to myeloid populations within the spleen that can express this chemokine [55], but it
484 may serve as a signal for mobilizing and recruiting bone marrow derived monocytes that
485 eventually infiltrate the injured spinal cord. Thus, the suppression of peripheral CCL2 by SRI-
486 42127 may further reduce the inflammatory milieu in the injured spinal cord.
487
488 IL-6 was induced both in liver and splenic tissues in conjunction with a very large increase in
489 circulating levels. In liver, IL-6 induction is a component of inflammation that has been observed

490 in animal models of acute SCI [49]. Selective induction of IL-6 in liver and spleen versus TNF-α
491 and IL-1β has been observed in other models of immune activation [56, 57] although the
492 mechanism remains unclear. Our findings do suggest, however, that these organs are major
493 contributors to circulating IL-6 in early SCI. In humans, elevated serum IL-6 has been detected
494 in the acute phase of SCI, with some studies correlating levels with clinical severity of injury (see
495 review [58]). The attenuation of systemic IL-6 by SRI-42127 may also have contributed to the
496 reduction in pain after SCI as discussed above. Taken together, the suppression of peripheral
497 inflammatory responses by SRI-42127 underscores the broad reach of HuR in cell types outside
498 of the CNS [4, 59].
499
500 The effectiveness of SRI-42127 in blocking the inflammatory cascade is borne out by the
501 significantly improved histological and behavioral outcomes. There was attenuation of microglial
502 activation in the injured spinal cord, and reduced lesion size with sparing of neurons and white
503 matter. Interestingly, we also observed a significant increase in myelin sparing in rostral and
504 caudal levels in SRI-treated mice. Loss of myelin in these levels is likely related to Wallerian
505 degeneration in long white matter tracts both rostral and caudal to injury, reflective of distal axonal
506 degeneration following separation of axons from their cell body [47, 60].
507
508 In our prior work, we found that SRI-42127 penetrates the CNS to therapeutic concentrations
509 within 10-15 minutes after systemic delivery [13] and rapidly suppresses neuroinflammatory
510 responses [10]. These are favorable features for clinical translation in acute SCI where “time is
511 spine” has emerged as a central theme in clinical management [6]. Because SRI-42127 can be
512 administered systemically, it could be given in the field by emergency personnel shortly after
513 injury. In our experimental paradigm, SRI-42127 was given 1 hour after SCI for a duration of 5
514 days.
515

516 Neuroinflammatory responses, including activated microglia and macrophages, persist in chronic
517 phases when their role switches to a restorative one, promoting neural plasticity, angiogenesis
518 and stem cell proliferation [3, 61, 62]. HuR regulates trophic factors that promote these restorative
519 functions such as Hif-1α, VEGF, and GM-CSF, so prolonged treatment with SRI-42127 may be
520 harmful [32, 59, 63-65]. Even IL-6 signaling may promote SCI recovery and neural regeneration
521 [58]. However, the major deleterious pro-inflammatory cytokines regulated by HuR, approach pre-
522 injury levels by 7 days, providing a time frame for intervention with HuR inhibitors. Further studies
523 will be required to delineate the optimal duration for SRI-42127 treatment after SCI.
524

525 **Abbreviations**

526

527 ARE: AU-rich elements

528 BL: Baseline

529 BMS: Basso mouse scale

530 BSCB: Blood-spinal cord barrier

531 CCL2: C-C Motif chemokine ligand 2

532 CCR2: C-C chemokine receptor type 2

533 COX-2: Cyclooxygenase-2

534 CXCL: chemokine (C-X-C motif) ligand

535 D: Drug (SRI-42127)

536 DAMPs: Damage-associated molecular patterns

537 DAPI: 4',6-diamidino-2-phenylindole

538 FI: Fluorescence intensity

539 GFAP: Glial fibrillary acidic protein

540 HuR: Human antigen R

541 Iba1 : Ionized calcium binding adaptor molecule 1

542 IL-6 : Interleukin 6

543 IL1-β : Interleukin-1 beta

544 iNOS : Inducible nitric oxide synthase

545 IP: intraperitoneal

546 LPS: Lipopolysaccharide

547 MGS: Mouse grimace scale

548 MMP: Matrix metalloproteinase

549 NeuN: Neuronal nuclei

550 PBS: Phosphate buffer saline

551 RBP: RNA binding protein

552 SCI: Spinal cord injury

553 Sh: Sham

554 SNI: Spared nerve injury

555 SRI: SRI-42127

556 TGF-β1: transforming growth factor beta-1

557 TNF-α: Tumor necrosis factor alpha

558 UTR: Untranslated region

559 V: Vehicle

560

561

562 **Ethics approval and consent to participate**

563 The animal study was reviewed and approved by the UAB Institutional Animal Care and Use
564 Committee and were carried out in accordance with relevant guidelines and regulations of the
565 National Research Council Guide for the Care and Use of Laboratory Animals.

566

567 **Consent for publication**

568 Not applicable

569

570 **Availability of data and materials**

571 The data that support the findings of this study are available on request from the corresponding
572 author. The data are not publicly available due to privacy or ethical restrictions.

573

574 **Competing interests**

575 The authors declare no competing interests.

576

Funding

This work was supported by merit reviews (BX005899, BX004419, and BX006244) from the Department of Veterans Affairs (PHK).

Authors' contributions

MAH, PHK, and CPC contributed to the conception and design of the study. MAH, RS, RES, AK, YS, AZH, KAS, and JD performed experiments and acquired data. AG, SAA, LBN, NF contributed to data analysis and interpretation. MAH and PHK prepared figures and drafted the manuscript. All authors read and approved the final manuscript.

Acknowledgements

We wish to thank the UAB Animal Behavioral Assessment Core Facility for assistance in testing mice. We also thank Carlos A. Toro, PhD for helpful discussions regarding methodology.

594 **References**

595

596 1. Alizadeh A, Dyck SM, Karimi-Abdolrezaee S: **Traumatic Spinal Cord Injury: An**
597 **Overview of Pathophysiology, Models and Acute Injury Mechanisms.** *Front Neurol*
598 2019, **10**.
599 2. Bennett J, J MD, Emmady PD: **Spinal Cord Injuries.** In *StatPearls (Internet).* Treasure
600 Island (FL): StatPearls Publishing LLC.; 2024
601 3. Hellenbrand DJ, Quinn CM, Piper ZJ, Morehouse CN, Fixel JA, Hanna AS: **Inflammation**
602 **after spinal cord injury: a review of the critical timeline of signaling cues and cellular**
603 **infiltration.** *J Neuroinflammation* 2021, **18:**284.
604 4. Guha A, Husain MA, Si Y, Nabors LB, Filippova N, Promer G, Smith R, King PH: **RNA**
605 **regulation of inflammatory responses in glia and its potential as a therapeutic target**
606 **in central nervous system disorders.** *Glia* 2023, **71:**485-508.
607 5. Kumar H, Ropper AE, Lee SH, Han I: **Propitious Therapeutic Modulators to Prevent**
608 **Blood-Spinal Cord Barrier Disruption in Spinal Cord Injury.** *Mol Neurobiol* 2017,
609 **54:**3578-3590.
610 6. Ahuja CS, Wilson JR, Nori S, Kotter MRN, Druschel C, Curt A, Fehlings MG: **Traumatic**
611 **spinal cord injury.** *Nature Reviews Disease Primers* 2017, **3:**17018.
612 7. Wang J, Leavenworth JW, Hjelmeland AB, Smith R, Patel N, Borg B, Si Y, King PH:
613 **Deletion of the RNA regulator HuR in tumor-associated microglia and macrophages**
614 **stimulates anti-tumor immunity and attenuates glioma growth.** *Glia* 2019, **67:**2424-
615 2439.
616 8. Matsye P, Zheng L, Si Y, Kim S, Luo W, Crossman DK, Bratcher PE, King PH: **HuR**
617 **promotes the molecular signature and phenotype of activated microglia:**

618 **Implications for amyotrophic lateral sclerosis and other neurodegenerative**
619 **diseases.** *Glia* 2017, **65:**945-963.
620 9. Kwan T, Floyd CL, Kim S, King PH: **RNA Binding Protein Human Antigen R Is**
621 **Translocated in Astrocytes following Spinal Cord Injury and Promotes the**
622 **Inflammatory Response.** *J Neurotrauma* 2017, **34:**1249-1259.
623 10. Chellappan R, Guha A, Si Y, Kwan T, Nabors LB, Filippova N, Yang X, Myneni AS,
624 Meesala S, Harms AS, King PH: **SRI-42127, a novel small molecule inhibitor of the**
625 **RNA regulator HuR, potently attenuates glial activation in a model of**
626 **lipopolysaccharide-induced neuroinflammation.** *Glia* 2022, **70:**155-172.
627 11. Kwan T, Floyd CL, Patel J, Mohaimany-Aponte A, King PH: **Astrocytic expression of**
628 **the RNA regulator HuR accentuates spinal cord injury in the acute phase.** *Neurosci*
629 *Lett* 2017, **651:**140-145.
630 12. Guo H, Du M, Yang Y, Lin X, Wang Y, Li H, Ren J, Xu W, Yan J, Wang N: **Sp1 regulates**
631 **the M1 polarization of microglia through the HuR/NF-κB axis after spinal cord injury.**
632 *Neuroscience* 2024.
633 13. Filippova N, Yang X, Ananthan S, Calano J, Pathak V, Bratton L, Vekariya RH, Zhang S,
634 Ofori E, Hayward EN, et al: **Targeting the HuR Oncogenic Role with a New Class of**
635 **Cytoplasmic Dimerization Inhibitors.** *Cancer Res* 2021, **81:**2220-2233.
636 14. Filippova N, Yang X, Ananthan S, Sorochinsky A, Hackney JR, Gentry Z, Bae S, King P,
637 Nabors LB: **Hu antigen R (HuR) multimerization contributes to glioma disease**
638 **progression.** *J Biol Chem* 2017, **292:**16999-17010.
639 15. Meisner NC, Hintersteiner M, Mueller K, Bauer R, Seifert JM, Naegeli HU, Ottl J, Oberer
640 L, Guenat C, Moss S, et al: **Identification and mechanistic characterization of low-**
641 **molecular-weight inhibitors for HuR.** *Nat Chem Biol* 2007, **3:**508-515.
642 16. Sorge RE, Si Y, Norian LA, Guha A, Moore GE, Nabors LB, Filippova N, Yang X, Smith
643 R, Chellappan R, King PH: **Inhibition of the RNA Regulator HuR by SRI-42127**

644 **Attenuates Neuropathic Pain After Nerve Injury Through Suppression of**
645 **Neuroinflammatory Responses.** *Neurotherapeutics* 2022, **19:**1649-1661.
646 17. Guida F, De Gregorio D, Palazzo E, Ricciardi F, Boccella S, Belardo C, Iannotta M,
647 Infantino R, Formato F, Marabese I, et al: **Behavioral, Biochemical and**
648 **Electrophysiological Changes in Spared Nerve Injury Model of Neuropathic Pain.** In
649 *Int J Mol Sci*, vol. 21, 2020/05/15 edition; 2020.
650 18. Ziebell JM, Adelson PD, Lifshitz J: **Microglia: dismantling and rebuilding circuits after**
651 **acute neurological injury.** *Metab Brain Dis* 2015, **30:**393-400.
652 19. Streit WJ, Walter SA, Pennell NA: **Reactive microgliosis.** *Prog Neurobiol* 1999, **57:**563-
653 581.
654 20. Basso DM, Fisher LC, Anderson AJ, Jakeman LB, McTigue DM, Popovich PG: **Basso**
655 **Mouse Scale for locomotion detects differences in recovery after spinal cord injury**
656 **in five common mouse strains.** *J Neurotrauma* 2006, **23:**635-659.
657 21. Ito S, Kakuta Y, Yoshida K, Shirota Y, Mieda T, Iizuka Y, Chikuda H, Iizuka H, Nakamura
658 K: **A simple scoring of beam walking performance after spinal cord injury in mice.**
659 *PLoS One* 2022, **17:**e0272233.
660 22. Langford DJ, Bailey AL, Chanda ML, Clarke SE, Drummond TE, Echols S, Glick S, Ingrao
661 J, Klassen-Ross T, Lacroix-Fralish ML, et al: **Coding of facial expressions of pain in**
662 **the laboratory mouse.** *Nat Methods* 2010, **7:**447-449.
663 23. Green TRF, Murphy SM, Rowe RK: **Comparisons of quantitative approaches for**
664 **assessing microglial morphology reveal inconsistencies, ecological fallacy, and a**
665 **need for standardization.** *Sci Rep* 2022, **12:**18196.
666 24. Reddaway J, Richardson PE, Bevan RJ, Stoneman J, Palombo M: **Microglial**
667 **morphometric analysis: so many options, so little consistency.** *Front Neuroinform*
668 2023, **17:**1211188.

669 25. Dixon DA, Tolley ND, King PH, Nabors LB, McIntyre TM, Zimmerman GA, Prescott SM:
670 **Altered expression of the mRNA stability factor HuR promotes cyclooxygenase-2**
671 **expression in colon cancer cells.** *J Clin Invest* 2001, **108:**1657-1665.
672 26. Cok SJ, Morrison AR: **The 3'-Untranslated Region of Murine Cyclooxygenase-2**
673 **Contains Multiple Regulatory Elements That Alter Message Stability and**
674 **Translational Efficiency.** *J Biol Chem* 2001, **276:**23179-23185.
675 27. Anthony DC, Couch Y: **The systemic response to CNS injury.** *Exp Neurol* 2014,
676 **258:**105-111.
677 28. Noble BT, Brennan FH, Popovich PG: **The spleen as a neuroimmune interface after**
678 **spinal cord injury.** *Journal of Neuroimmunology* 2018, **321:**1-11.
679 29. Sterner RC, Sterner RM: **Immune response following traumatic spinal cord injury:**
680 **Pathophysiology and therapies.** *Front Immunol* 2022, **13:**1084101.
681 30. Anwar MA, Al Shehabi TS, Eid AH: **Inflammogenesis of Secondary Spinal Cord Injury.**
682 *Front Cell Neurosci* 2016, **10:**98.
683 31. Moraga I, Spangler J, Mendoza JL, Garcia KC: **Multifarious determinants of cytokine**
684 **receptor signaling specificity.** *Adv Immunol* 2014, **121:**1-39.
685 32. Guha A, Waris S, Nabors LB, Filippova N, Gorospe M, Kwan T, King PH: **The versatile**
686 **role of HuR in Glioblastoma and its potential as a therapeutic target for a multi-**
687 **pronged attack.** *Adv Drug Deliv Rev* 2022, **181:**114082.
688 33. Bonomo I, Assoni G, La Pietra V, Canarutto G, Facen E, Donati G, Zucal C, Genovese S,
689 Micaelli M, Pérez-Ràfols A, et al: **HuR modulation with tanshinone mimics impairs**
690 **LPS response in murine macrophages.** *Disease Models & Mechanisms* 2023.
691 34. Guptarak J, Wanchoo S, Durham-Lee J, Wu Y, Zivadinovic D, Paulucci-Holthauzen A,
692 Nesic O: **Inhibition of IL-6 signaling: A novel therapeutic approach to treating spinal**
693 **cord injury pain.** *Pain* 2013, **154:**1115-1128.

694 35. Murakami T, Kanchiku T, Suzuki H, Imajo Y, Yoshida Y, Nomura H, Cui D, Ishikawa T,
695 Ikeda E, Taguchi T: **Anti-interleukin-6 receptor antibody reduces neuropathic pain**
696 **following spinal cord injury in mice.** *Exp Ther Med* 2013, **6:**1194-1198.
697 36. Lee JY, Park CS, Seo KJ, Kim IY, Han S, Youn I, Yune TY: **IL-6/JAK2/STAT3 axis**
698 **mediates neuropathic pain by regulating astrocyte and microglia activation after**
699 **spinal cord injury.** *Exp Neurol* 2023, **370:**114576.
700 37. Ji H, Zhang Y, Chen C, Li H, He B, Yang T, Sun C, Hao H, Zhang X, Wang Y, et al: **D-**
701 **dopachrome tautomerase activates COX2/PGE(2) pathway of astrocytes to mediate**
702 **inflammation following spinal cord injury.** *J Neuroinflammation* 2021, **18:**130.
703 38. Chelluboina B, Nalamolu KR, Klopfenstein JD, Pinson DM, Wang DZ, Vemuganti R,
704 Veeravalli KK: **MMP-12, a Promising Therapeutic Target for Neurological Diseases.**
705 *Mol Neurobiol* 2018, **55:**1405-1409.
706 39. Wang J, Hjelmeland AB, Nabors LB, King PH: **Anti-cancer effects of the HuR inhibitor,**
707 **MS-444, in malignant glioma cells.** *Cancer Biol Ther* 2019, **20:**979-988.
708 40. Li Q, Yang Z, Wang K, Chen Z, Shen H: **Suppression of microglial Ccl2 reduces**
709 **neuropathic pain associated with chronic spinal compression.** *Front Immunol* 2023,
710 **14:**1191188.
711 41. Thacker MA, Clark AK, Bishop T, Grist J, Yip PK, Moon LD, Thompson SW, Marchand F,
712 McMahon SB: **CCL2 is a key mediator of microglia activation in neuropathic pain**
713 **states.** *Eur J Pain* 2009, **13:**263-272.
714 42. Ma M, Wei T, Boring L, Charo IF, Ransohoff RM, Jakeman LB: **Monocyte recruitment**
715 **and myelin removal are delayed following spinal cord injury in mice with CCR2**
716 **chemokine receptor deletion.** *Journal of Neuroscience Research* 2002, **68:**691-702.
717 43. Abbadie C, Lindia JA, Cumiskey AM, Peterson LB, Mudgett JS, Bayne EK, DeMartino JA,
718 MacIntyre DE, Forrest MJ: **Impaired neuropathic pain responses in mice lacking the**
719 **chemokine receptor CCR2.** *Proc Natl Acad Sci U S A* 2003, **100:**7947-7952.

720 44. Banisadr G, Quéraud-Lesaux F, Boutterin MC, Pélaprat D, Zalc B, Rostène W, Haour F,
721 Mélik Parsadaniantz S: **Distribution, cellular localization and functional role of CCR2**
722 **chemokine receptors in adult rat brain.** *Journal of Neurochemistry* 2002, **81:**257-269.
723 45. Joko M, Osuka K, Usuda N, Atsuzawa K, Aoyama M, Takayasu M: **Different**
724 **modifications of phosphorylated Smad3C and Smad3L through TGF-beta after**
725 **spinal cord injury in mice.** *Neurosci Lett* 2013, **549:**168-172.
726 46. Gong L, Gu Y, Han X, Luan C, Liu C, Wang X, Sun Y, Zheng M, Fang M, Yang S, et al:
727 **Spatiotemporal Dynamics of the Molecular Expression Pattern and Intercellular**
728 **Interactions in the Glial Scar Response to Spinal Cord Injury.** *Neurosci Bull* 2023,
729 **39:**213-244.
730 47. Shafqat A, Albalkhi I, Magableh HM, Saleh T, Alkattan K, Yaqinuddin A: **Tackling the**
731 **glial scar in spinal cord regeneration: new discoveries and future directions.** *Front*
732 *Cell Neurosci* 2023, **17:**1180825.
733 48. Ma CW, Wang ZQ, Ran R, Liao HY, Lyu JY, Ren Y, Lei ZY, Zhang HH: **TGF-β signaling**
734 **pathway in spinal cord injury: Mechanisms and therapeutic potential.** *J Neurosci Res*
735 2024, **102:**e25255.
736 49. Goodus MT, McTigue DM: **Hepatic dysfunction after spinal cord injury: A vicious**
737 **cycle of central and peripheral pathology?** *Exp Neurol* 2020, **325:**113160.
738 50. Yates AG, Jogia T, Gillespie ER, Couch Y, Ruitenberg MJ, Anthony DC: **Acute IL-1RA**
739 **treatment suppresses the peripheral and central inflammatory response to spinal**
740 **cord injury.** *Journal of Neuroinflammation* 2021, **18:**15.
741 51. Campbell SJ, Perry VH, Pitossi FJ, Butchart AG, Chertoff M, Waters S, Dempster R,
742 Anthony DC: **Central nervous system injury triggers hepatic CC and CXC chemokine**
743 **expression that is associated with leukocyte mobilization and recruitment to both**
744 **the central nervous system and the liver.** *Am J Pathol* 2005, **166:**1487-1497.

745 52. Campbell SJ, Hughes PM, Iredale JP, Wilcockson DC, Waters S, Docagne F, Perry VH,
746 Anthony DC: **CINC-1 is an acute-phase protein induced by focal brain injury causing**
747 **leukocyte mobilization and liver injury.** *Faseb j* 2003, **17:**1168-1170.
748 53. D'Mello C, Le T, Swain MG: **Cerebral microglia recruit monocytes into the brain in**
749 **response to tumor necrosis factoralpha signaling during peripheral organ**
750 **inflammation.** *J Neurosci* 2009, **29:**2089-2102.
751 54. Blomster LV, Brennan FH, Lao HW, Harle DW, Harvey AR, Ruitenberg MJ: **Mobilisation**
752 **of the splenic monocyte reservoir and peripheral CX3CR1 deficiency adversely**
753 **affects recovery from spinal cord injury.** *Experimental Neurology* 2013, **247:**226-240.
754 55. Gschwandtner M, Derler R, Midwood KS: **More Than Just Attractive: How CCL2**
755 **Influences Myeloid Cell Behavior Beyond Chemotaxis.** *Frontiers in Immunology* 2019,
756 **10**.
757 56. Szot P, Franklin A, Figlewicz DP, Beuca TP, Bullock K, Hansen K, Banks WA, Raskind
758 MA, Peskind ER: **Multiple lipopolysaccharide (LPS) injections alter interleukin 6 (IL-**
759 **6), IL-7, IL-10 and IL-6 and IL-7 receptor mRNA in CNS and spleen.** *Neuroscience*
760 2017, **355:**9-21.
761 57. Zhu XL, Pacheco ND, Dick EJ, Rollwagen FM: **Differentially increased IL-6 mRNA**
762 **expression in liver and spleen following injection of liposome-encapsulated**
763 **haemoglobin.** *Cytokine* 1999, **11:**696-703.
764 58. Shipman H, Monsour M, Foley MM, Marbacher S, Croci DM, Bisson EF: **Interleukin-6 in**
765 **Spinal Cord Injury: Could Immunomodulation Replace Immunosuppression in the**
766 **Management of Acute Traumatic Spinal Cord Injuries?** *J Neurol Surg A Cent Eur*
767 *Neurosurg* 2024.
768 59. Srikantan S, Gorospe M: **HuR function in disease.** *Front Biosci (Landmark Ed)* 2012,
769 **17:**189-205.

770 60. Cohen-Adad J, Leblond H, Delivet-Mongrain H, Martinez M, Benali H, Rossignol S:
771 **Wallerian degeneration after spinal cord lesions in cats detected with diffusion**
772 **tensor imaging.** *Neuroimage* 2011, **57:**1068-1076.
773 61. Wu Y, Tang Z, Zhang J, Wang Y, Liu S: **Restoration of spinal cord injury: From**
774 **endogenous repairing process to cellular therapy.** *Front Cell Neurosci* 2022,
775 **16:**1077441.
776 62. Freyermuth-Trujillo X, Segura-Uribe JJ, Salgado-Ceballos H, Orozco-Barrios CE, Coyoy-
777 Salgado A: **Inflammation: A Target for Treatment in Spinal Cord Injury.** *Cells* 2022,
778 **11**.
779 63. Li Y, Han W, Wu Y, Zhou K, Zheng Z, Wang H, Xie L, Li R, Xu K, Liu Y, et al: **Stabilization**
780 **of Hypoxia Inducible Factor-1alpha by Dimethyloxalylglycine Promotes Recovery**
781 **from Acute Spinal Cord Injury by Inhibiting Neural Apoptosis and Enhancing Axon**
782 **Regeneration.** *J Neurotrauma* 2019, **36:**3394-3409.
783 64. Zamanian C, Kim G, Onyedimma C, Ghaith AK, Jarrah R, Graepel S, Moinuddin FM,
784 Bydon M: **A review of vascular endothelial growth factor and its potential to improve**
785 **functional outcomes following spinal cord injury.** *Spinal Cord* 2023, **61:**231-237.
786 65. Tao JW, Fan X, Zhou JY, Huo LY, Mo YJ, Bai HZ, Zhao Y, Ren JP, Mu XH, Xu L:
787 **Granulocyte colony-stimulating factor effects on neurological and motor function**
788 **in animals with spinal cord injury: a systematic review and meta-analysis.** *Front*
789 *Neurosci* 2023, **17:**1168764.
790

791 Figure Legends

792 **Figure 1: SRI-42127 attenuates motor function loss and pain after SCI.** Following SCI, SRI-
793 42127 (10mg/kg) or vehicle was administered IP at 6 h intervals for 5 days starting 1 h after
794 injury. **(A)** BMS scores for vehicle control and SRI-treated mice were measured at 1, 2 and 3
795 weeks after SCI. **(B)** Motor function post SCI was assessed by open field testing. A representative
796 heat map of activity at 2 weeks post SCI is shown. Different parameters of motor activity were
797 measured including **(C)** distance moved, **(D)** mobility**,** and **(E)** velocity. **(F)** Beam walking scores
798 of vehicle and SRI-treated mice were obtained at 1, 2, 3 weeks post SCI. **(G)** Rotarod testing was
799 performed at 1-, 2- and 3-weeks post SCI and latency to fall was measured. **(H)** Non-evoked pain
800 was assessed by mouse grimace scores (MGS) which were measured at day 2 and 9 post SCI.
801 Baseline testing of both test groups, prior to SCI, had similar MGS scores. Evaluations for open
802 field BMS, beam walking, and non-evoked pain were made by two observers blinded to the status
803 of the animal. Error bars represent means ± SD of 6 mice/group. P values: * < 0.05, ** < 0.01, ***
804 < 0.001, **** < 0.0001.

805

806 **Figure 2: SRI-42127 treatment reduces lesion size and loss of neurons after SCI while**
807 **increasing myelin sparing. (A)** Representative GFAP-immunostained sections from the
808 epicenter (3 weeks post SCI) showing reduced lesion size in an SRI-treated mouse compared to
809 vehicle control. **(B)** Total lesion area was quantified in 3 vehicle and 3 SRI-treated mice. **(C)**
810 Representative NeuN-immunostained sections from the epicenter showing an increase in NeuN+
811 cells in the SRI-treated mouse. **(D)** NeuN+ cells were quantified at the epicenter in 3 vehicle and
812 3 SRI-treated mice at 3 weeks post-SCI. **(E)** NeuN fluorescence intensity (FI) was quantified at
813 the epicenter. **(F)** Representative fluoromyelin-stained sections from the epicenter showing
814 increased myelin staining in SRI-treated mouse compared to vehicle control. **(G)** Fluoromyelin
815 staining at the epicenter was quantified in 3 vehicle and 3 SRI-treated mice. Dashed lines

816 delineate the boundary of injured spinal cord. Bars represent the mean ± SD of 3 mice/group. P
817 < **0.01. Scale bars 100 μm.
818
819 **Figure 3**: **SRI-42127 inhibits nucleocytoplasmic translocation of HuR in microglia and**
820 **attenuates microglial activation**. Eight hours after SCI, sections from the epicenter were
821 immunostained with antibodies as shown. **(A)** Cytoplasmic translocation of HuR is observed in
822 microglia at the epicenter from a vehicle treated mouse as indicated by a merged yellow signal of
823 HuR and Iba1 (arrow heads). A higher power view of a microglial cell (white arrow) is shown in
824 the insert. **(B)** SRI-42127 treatment blocked HuR translocation from the nucleus as indicated by
825 a merged signal of HuR, Iba1 and nuclear DAPI as well as an absence of a merged yellow signal.
826 A higher power view of a microglial cell (white arrow) is shown in the insert. **(C)** Microglial HuR
827 localization was quantified in 5 cells from 3 biological replicates as described in the Methods and
828 expressed as a nuclear/cytoplasmic ratio. **(D)** Quantification of Iba1 fluorescence intensity (FI) in
829 11-13 cells from 3 biological replicates. **(E)** Total Iba1 FI was quantified at the epicenter, rostral,
830 and caudal levels. **(F)** Total Iba1+ cell counts at the epicenter were quantified in 3 biological
831 replicates. P * < .05, P < **0.01, *** < 0.001, **** < .0001. Scale bars 50 μm, 10 μm (inserts).
832
833 **Figure 4: SRI-42127 attenuates activation-associated changes in microglial morphology**
834 **after SCI. (A)** Eight hours after SCI, tissue sections from the epicenter were immunostained with
835 Iba1 antibodies and digitally converted to Skeletonized images using Fiji software. Representative
836 images are shown. Morphological features were quantified including total microglia branch length,
837 number of branches per microglial cell**,** and number of branch endpoints per microglial cell. Data
838 were generated from 5007 microglial cells from vehicle control (n = 3 biological replicates) and
839 4538 microglial cells from SRI (n=3 biological replicates). **(B)** The soma of Iba1+ microglial cells
840 were identified as shown in the representative images to the left. Binary images were generated

841 by adjusting the Fiji threshold level (shown in inserts). Total area was quantified in 11 cells from
842 3 biological replicates as shown in the graph. Error bars represent SD. P *** < 0.001, **** < .0001.
843
844 **Figure 5: SRI-42127 attenuates pro-inflammatory cytokine and chemokine mRNA induction**
845 **(A)** Spinal cords were harvested at 8 h post-SCI and divided into 3 segments: injury epicenter,
846 rostral and caudal. RNA expression of proinflammatory cytokines and chemokines was assessed
847 by qPCR in vehicle controls and SRI treated mice. All values were expressed relative to the
848 vehicle control which was set at 1.0. GAPDH was used as the housekeeping control. P values: *
849 < 0.05, ** < 0.01, *** < 0.001, **** < 0.0001. Error bars represent means ± SEM of 6 mice/group.
850 **(B)** COX-2 western blot of protein lysate from epicenter, rostral and caudal spinal cord levels
851 obtained 8 h after SCI. A representative blot is shown above. COX-2 levels were quantified by
852 densitometry from three biological replicates using vinculin as a loading control. All values were
853 expressed relative to the vehicle controls at rostral and caudal segments which were set at 1.0.
854 Error bars represent the mean ± SD. P values: * < 0.05.
855
856 **Figure 6: SRI-42127 suppresses expression of pro-inflammatory mediators peripherally**.
857 **(A)** ELISA was used to quantify cytokines in plasma samples obtained at 8 h post SCI or sham
858 injury (Sh). **(B)** At the same time interval, RNA was harvested from liver and spleen and assessed
859 by qPCR for *CXCL1*, *CCL2*, and *IL-6* mRNA expression. Data represent the mean ± SD of 6
860 mice/group in plasma and ± SD of 3 mice/group in liver and spleen. P values: ** < 0.01, *** <
861 0.001, **** < 0.0001.
862
863
864 **Supplementary Figure 1: Behavioral assessment in sham mice.** Mice were subjected to
865 sham injury and then given vehicle or SRI-42127 every 6 hours for 5 days. **(A)** Open field BMS
866 score heatmap, total distance travelled, velocity, and mobility show no difference in motor

867 activity between vehicle- and SRI-treated mice **(B)** Balance beam test score showed no deficits
868 in vehicle or SRI-treated mice.

869

870 **Supplementary Figure 2: Assessment of caudal and rostral sections of spinal cord from**
871 **vehicle and SRI-treated mice.** At 3 weeks post SCI, rostral and caudal segments of 3 vehicle
872 and 3 SRI-treated mice were evaluated by immunohistochemistry. **(A)** GFAP staining shows no
873 evidence of glial scarring. **(B)** NeuN staining shows equal neuronal counts in vehicle and SRI-
874 treated mice. **(C)** Fluoromyelin staining shows a significant increase in myelin in SRI-treated mice.
875 P value: ** < 0.01.

876

877 **Supplementary Figure 3: HuR nucleocytoplasmic translocation was not observed in**
878 **microglia in uninjured spinal cord levels.** Caudal or rostral segments of vehicle- and SRI-
879 treated mice were assessed for HuR localization after SCI and showed no evidence of
880 nucleocytoplasmic translocation.

881

882 **Supplementary Figure 4: HuR nucleocytoplasmic translocation in astrocytes is delayed**
883 **after SCI and blocked by SRI-42127.** At 8 and 24 h after SCI, sections from the epicenter of
884 vehicle and SRI-treated mice were immunostained with HuR and GFAP antibodies as shown. (A)
885 At 8 h, HuR remained nuclear in location. (B) At 24 h, there is translocation of HuR in a vehicle-
886 treated mouse as indicated by arrows (upper panels) which is blocked by SRI-42127 treatment
887 (lower panels)**.** Scale bars, 10 μm, 50 μm.

888

889 **Supplementary Figure 5: Suppression of pro-inflammatory cytokines persists after 5 days**
890 At 5 days after SCI, the epicenter of injured mice receiving vehicle or SRI-42127 was assessed

891 for inflammatory mediator expression by qPCR. P values: ** < 0.01, **** < 0.0001. Error bars
892 represent the mean ± SD of 3 mice/group.
893
894 **Supplementary Figure 6: Cytokines which had minimal or no mRNA induction in peripheral**
895 **tissues.** At 8 h after SCI or sham injury, total RNA from liver and spleen was assessed by qPCR
896 for expression of the inflammatory mediators shown. P value: * < 0.05. Error bars represent the
897 mean ± SD of 3 mice/group.
898
899 **Supplementary Figure 7: Unedited western blot of COX-2 and vinculin loading control**
900 **from Figure 5B.**

Fig 1

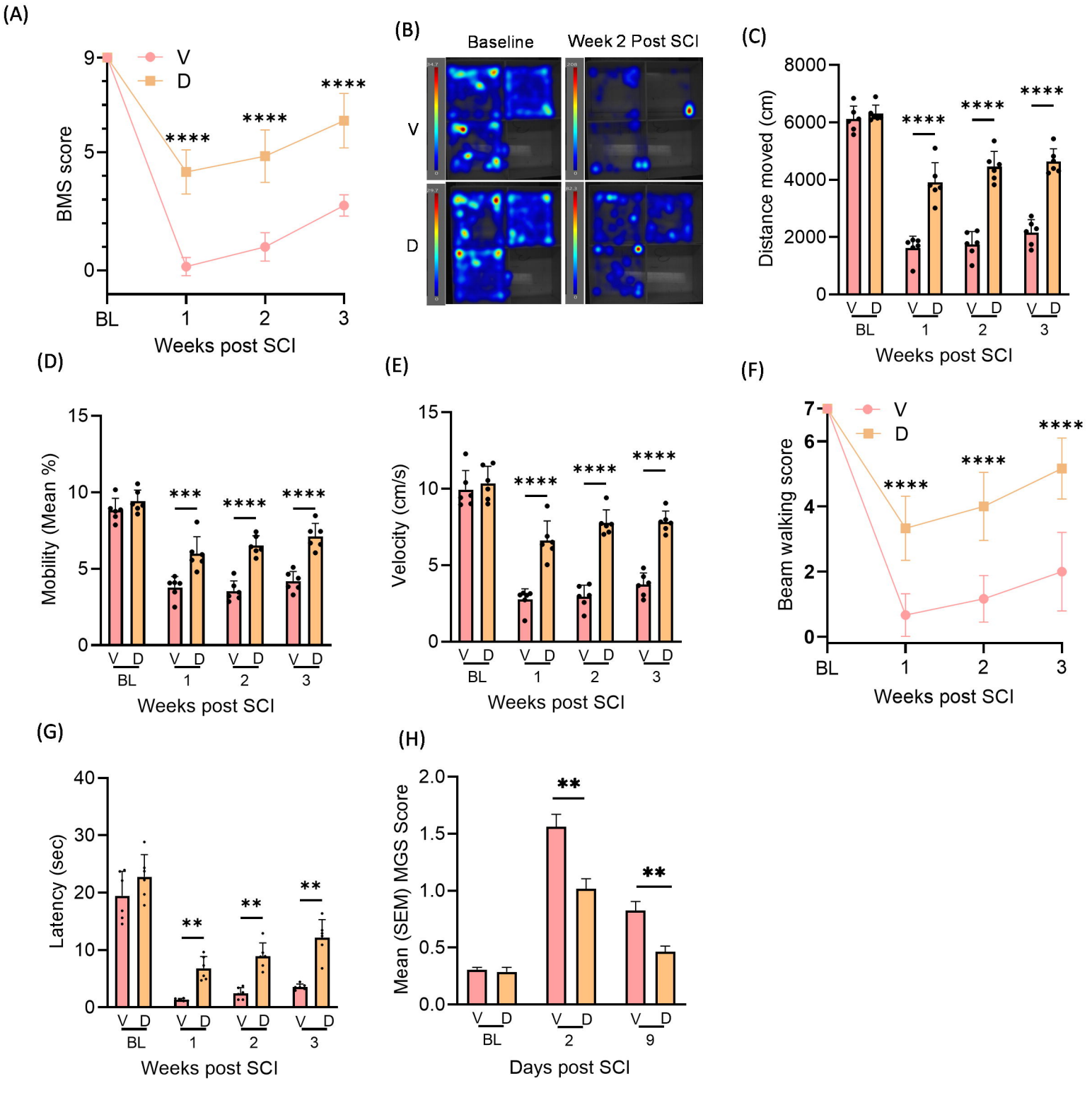
(A)
V
D
BMS score
Weeks post SCI
BL
1
2
3
****
(B)
Baseline
Week 2 Post SCI
V
D
(C)
Distance moved (cm)
Weeks post SCI
(D)
Mobility (Mean %)
Weeks post SCI
(E)
Velocity (cm/s)
Weeks post SCI
(F)
Beam walking score
Weeks post SCI
(G)
Latency (sec)
Weeks post SCI
(H)
Mean (SEM) MGS Score
Days post SCI
**
***

Fig 2

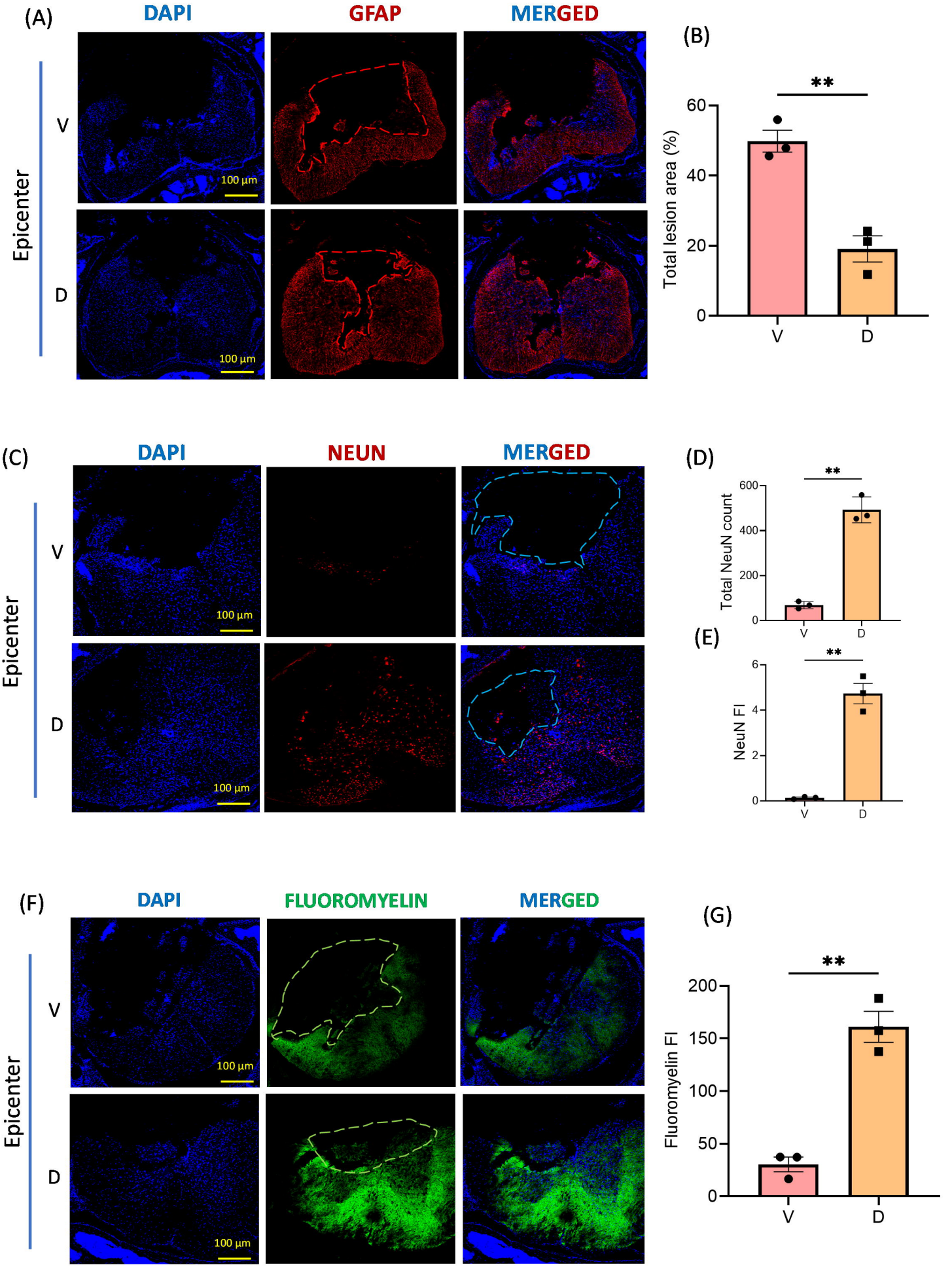
(A)
DAPI
GFAP
MERGED
Epicenter
V
D
100 µm
(B)
**
Total lesion area (%)
60
40
20
0
V
D
(C)
DAPI
NEUN
MERGED
Epicenter
V
D
100 µm
(D)
**
Total NeuN count
600
400
200
0
V
D
(E)
**
NeuN FI
6
4
2
0
V
D
(F)
DAPI
FLUOROMYELIN
MERGED
Epicenter
V
D
100 µm
(G)
**
Fluoromyelin FI
200
150
100
50
0
V
D

Fig 3

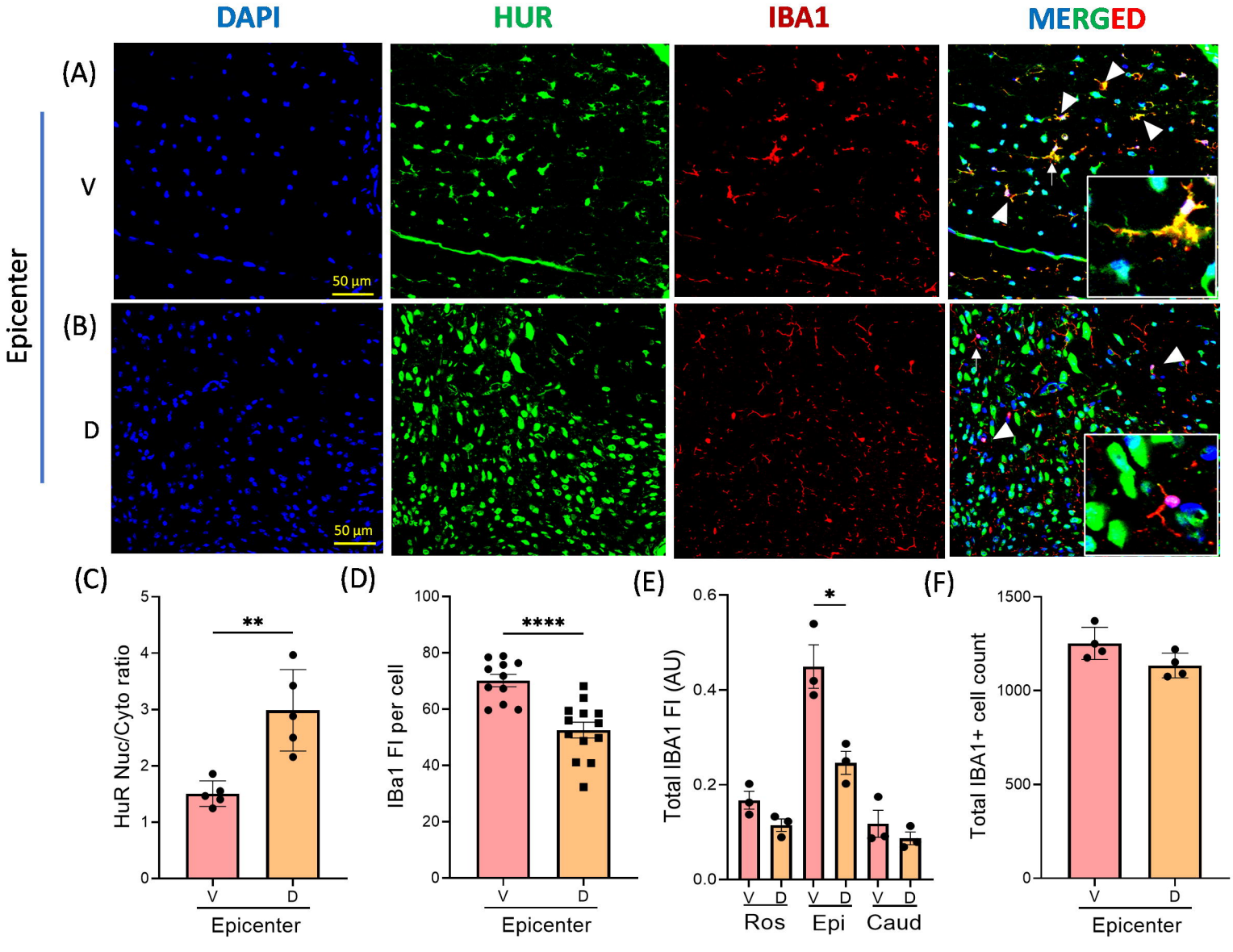
DAPI
HUR
IBA1
MERGED
(A)
V
(B)
D
Epicenter
50 µm
50 µm
(C)
HuR Nuc/Cyto ratio
**
V
D
Epicenter
(D)
IBa1 FI per cell
****
V
D
Epicenter
(E)
Total IBA1 FI (AU)
*
V D V D V D
Ros Epi Caud
(F)
Total IBA1+ cell count
V
D
Epicenter

Fig 4

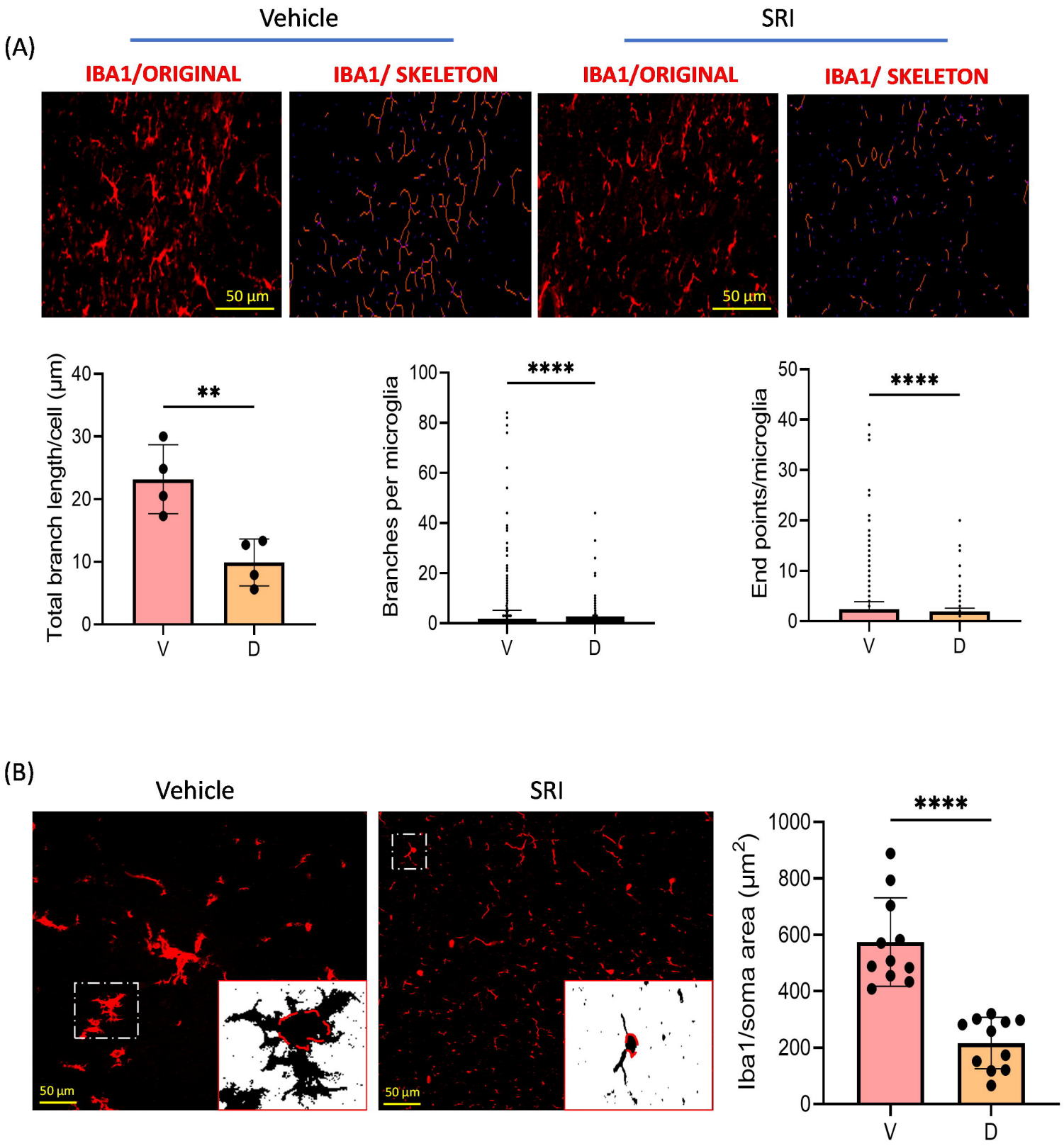
(A)
Vehicle
SRI
IBA1/ORIGINAL
IBA1/ SKELETON
IBA1/ORIGINAL
IBA1/ SKELETON
50 µm
50 µm
Total branch length/cell (µm)
**
Branches per microglia
****
End points/microglia
****
V
D
(B)
Vehicle
SRI
50 µm
50 µm
Iba1/soma area (µm²)
****
V
D

Fig 5

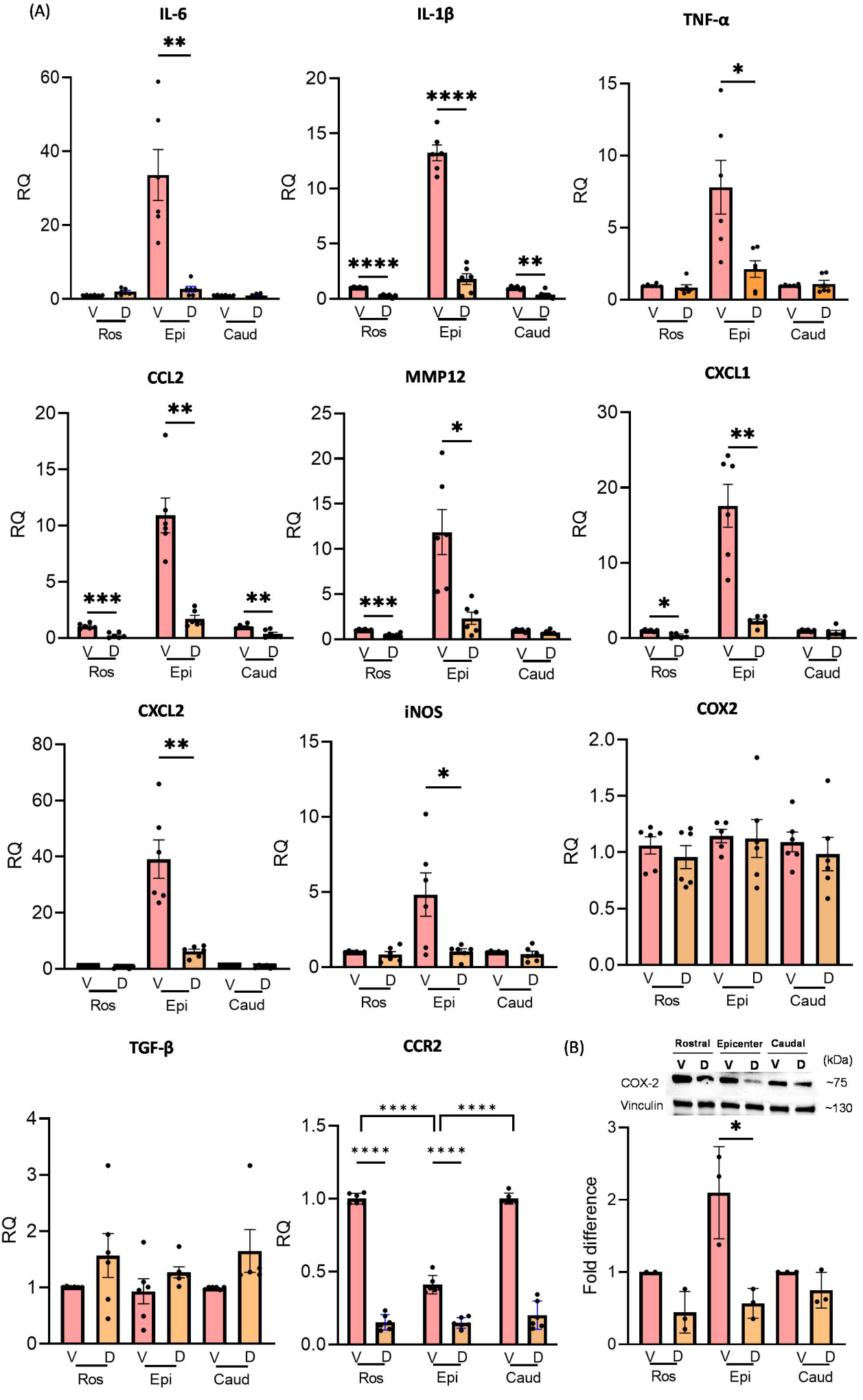
(A)
IL-6
IL-1β
TNF-α
CCL2
MMP12
CXCL1
CXCL2
iNOS
COX2
TGF-β
CCR2
RQ
V D
Ros
Epi
Caud
(B)
Rostral
Epicenter
Caudal
(kDa)
COX-2
Vinculin
~75
~130
Fold difference

Fig 6

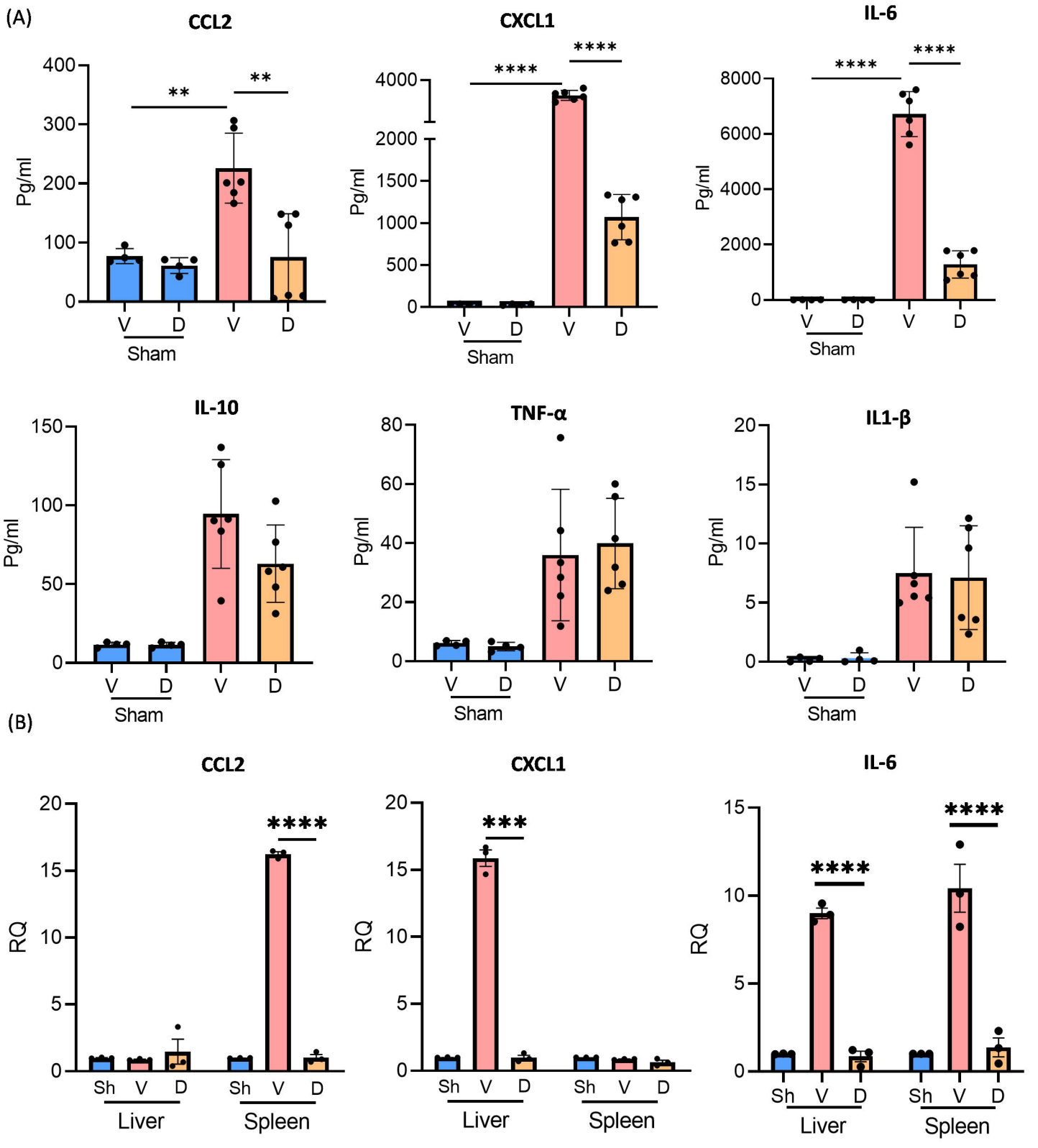
(A)
CCL2
CXCL1
IL-6
IL-10
TNF-α
IL1-β
Pg/ml
V
D
Sham
**
****
(B)
RQ
Sh
Liver
Spleen
***